Check for updates

Lead-free cesium tin halide nanocrystals for light-emitting diodes and color down conversion†

K. P. O. Mahesh,‡*[a] Che-Yu Chang,‡[b] Wei-Li Hong,[c] Tzu-Hsiang Wen,[a]
Pei-Hsuan Lo,[a] Hao-Zhe Chiu,[a] Ching-Ling Hsu,[b] Sheng-Fu Horng[c]
and Yu-Chiang Chao [ID] *[a]

Organometal halide perovskites are attracting a great deal of attention because of their long carrier diffusion lengths, wide wavelength tunability, and narrow-band emission. However, the toxicity of lead has caused considerable environmental and health concerns. In this work, lead-free cesium tin halide nanocrystals are synthesized and investigated. $CsSnBr_3$ and $CsSnI_3$ nanocrystals, 25 and 7 nm in size, are synthesized by a facile hot injection method. Absorption spectroscopy, photoluminescence spectroscopy, and X-ray diffraction were used to understand their structural and optical properties. $CsSnBr_3$ and $CsSnI_3$ nanocrystals show emission peaks at 683 and 938 nm, respectively. These nanocrystals show shelf stability for a few months. Temperature-dependent photoluminescence is utilized to know more about fundamental physical parameters, such as exciton binding energy, charge carrier–phonon interactions and band gap. Light-emitting diodes and color down-conversion films are also demonstrated using these lead free perovskite nanocrystals.

1. Introduction

Solution-processable perovskite semiconductors have drawn tremendous attention in the field of solar cells,[1] light-emitting diodes (LEDs),[2] color converters[3] and lasers.[4] In the past few years, LEDs based on colloidal all inorganic cesium lead halide ($CsPbX_3$, X = I⁻, Br⁻, and Cl⁻) quantum dots and nanoparticles have been broadly explored because of their tunable emission and high photoluminescence quantum yield.[5–8] The emission covers the entire visible spectral region that could be changed by controlling the chemical composition of halides and sizes of the nanoparticles. However, due to the health and environmental concerns, despite the impressive performance of $CsPbX_3$ have been demonstrated, the presence of toxic heavy metal, Pb, is a major difficulty towards the large-scale commercialization.

To replace Pb, perovskite materials with nontoxic metals such as tin, bismuth, and germanium have been investigated. Recently, the synthesis of nanostructured lead-free cesium tin halide perovskite quantum dots have been reported.[9–12] The

[a]Department of Physics, National Taiwan Normal University, Taipei, Taiwan 11677, Republic of China. E-mail: kpomahesh@gmail.com; ycchao@ntnu.edu.tw

[b]Department of Physics, Chung Yuan Christian University, Chung-Li, Taiwan 32023, Republic of China

[c]Institute of Electronics Engineering, National Tsing Hua University, Hsinchu, Taiwan 300, Republic of China

† Electronic supplementary information (ESI) available. See DOI: 10.1039/d0ra06139e

‡ K. P. O. Mahesh and Che-Yu Chang contributed equally to this work.

band gap was tuned by using different halides. Mixed halide perovskite quantum dots have been synthesized by either direct synthesis of different halide precursors or mixing of as-synthesized two different pure-halide perovskite quantum dots solution by anion exchange reaction. $CsSnX_3$ (X = I⁻, Br⁻, and Cl⁻) quantum rods were also synthesized by the solvothermal process.[13] The $CsSnX_3$ have been used not only for solar cells,[14–17] but also for the fabrication of LEDs.[18]

When comparing the LED, color conversion and solar cell applications using hybrid halide perovskite QDs, the optical properties of these QDs has been less investigated. To date, most research available on the optical properties of lead-free halide perovskite at room temperature.[19,20] A very few works have been reported on the steady-state PL characterization of $CsSnX_3$ QDs at less than 300 K.[21] The low temperature steady-state PL gives the in-depth information on electron–phonon interaction of hybrid halide QDs and thermal contribution to band gap of hybrid halide perovskite QDs.[22]

Here, we demonstrate a facile hot injection solution synthesis of monodisperse $CsSnBr_3$ and $CsSnI_3$ nanocrystals with 25 and 7 nm in size, respectively. $CsSn(Br_xI_{1-x})_3$ can also be realized by tuning the ratio of SnI_2 and $SnBr_2$. The structural and optical properties were investigated by absorption and photoluminescence spectroscopy, X-ray diffraction and transmission electron microscopy. We mainly focused on the steady-state PL spectra of $CsSnBr_3$ and $CsSnI_3$ nanocrystals in the broad temperature range between 80 K and 300 K. The temperature-dependent PL was used to investigate the exciton binding energy, charge carriers–phonon interaction and band

gap. As the temperature increases, the PL peak shows a linear blue-shift, the PL spectra's full width at half maximum (FWHM) shows a broadening characteristic, and the integrated PL intensity shows a continuous decrease. Increasing trend of binding energy was extracted by fitting to the temperature-dependent PL excitonic emission intensity. Besides, to demonstrate the possibility of these materials to be used in real applications, LEDs and color down-conversion films were realized based on these nanocrystals.

2. Experimental

2.1 Materials

For the synthesis and fabrication of $CsSnX_3$ and LEDs, analytical grade reagents were used as received without further purification.

2.2 Synthesis $CsSnX_3$ nanocrystals

The lead-free $CsSn(Br_xI_{1-x})_3$ nanocrystals was prepared by a facile hot injection method following the reported literature.[9] The preparation was conducted under nitrogen atmosphere by adopting the standard Schlenk line technique. Take a mixture of 0.696 g $SnBr_2$ or 0.931 g SnI_2 and 2.5 mL tri-n-octylphosphine (TOP) in a three-neck flask and heated to 100 °C with stirring for 1 hour under vacuum. In a separate three-neck flask, 0.13 g Cs_2CO_3, 12 mL octadecane (ODE), 0.55 mL oleic acid (OA) and 0.4 mL oleylamine (OLA) was stirred at 120 °C for 1 hour under vacuum and increases the temperature to 140 °C for one hour in N_2 atmosphere. Then the reaction temperature was increased to 170 °C in the presence of N_2. The SnX_2–TOP solution was quickly injected with effective stirring for 1 minute then cooled by an ice-cooled water bath. The $CsSnBr_3$ and $CsSnI_3$ nanocrystals are separated by centrifugation and washed three times with ethanol and hexane in a glove box.

2.3 Fabrication of color converters

The down-conversion films are fabricated using PMMA as a matrix. 25 mg of $CsSnBr_3$ or $CsSnI_3$ perovskite nanocrystals were dispersed in 1 mL of toluene, and 50 mg of PMMA is dissolved in 4 mL of toluene at 60 °C in a different vial. The $CsSnBr_3$ or $CsSnI_3$ toluene solutions are mixed with PMMA toluene solution under vigorous stirring for 30 min. Subsequently, the mixed solutions are transferred into a Petri-dish followed by placing into a vacuum oven for 30 min at room temperature for evaporating the toluene to get nanocrystals encapsulated PMMA composite film. The as-prepared nanocrystals/PMMA composites film is placed on top of a blue-emitting LED chip (455 nm) for the PL measurement.

2.4 Fabrication of LEDs

The light-emitting devices were fabricated on patterned indium tin oxide (ITO) glass substrates. The ITO glass substrates were cleaned by acetone, isopropanol, and de-ionized water and blown dry by nitrogen. After ultraviolet-ozone treatment for 30 min, the hole injection material poly(3,4-ethylenedioxythiophene):poly(styrene sulfonate) (PEDOT:PSS, Clevios P VP AI4083) was spin-coated

onto the substrates and baked at 120 °C for 20 min. The substrates were then transferred to a N_2-filled glovebox for the following fabrication processes. A blend solution consisting of poly(N-vinyl carbazole) (PVK), 2-(4-$tert$-butylphenyl)-5-(4-biphenylyl)-1,3,4-oxadiazole (PBD), N,N'-bis(3-methylphenyl)-N,N'-diphenylbenzidine (TPD), and $CsSnI_3$ nanocrystals was spin-coated at 1000 rpm on the substrates to form the emissive layer. PVK, PBD, and TPD were first prepared in toluene with a concentration of 2 wt%. A mixture was then prepared by blending 0.61 mL, 0.24 mL and 0.09 mL of PVK, PBD and TPD solutions together. The mixture was then used to prepare nanocrystal solution with a concentration of 70.85 mg mL^{-1}. The emissive layer was then annealed at 60 °C for 20 min to dry the film. LiF of 1.2 nm and Al of 70 nm were finally deposited as cathode to complete the devices.

2.5 Measurements

XRD data were recorded using a Bruker D8 ADVANCE ECO diffractometer (Cu Kα radiation, $\lambda = 0.15418$ nm). The absorbance spectra of the perovskite films were recorded using a microspectrometer (SD1200-LS-HA, StreamOptics Co.) with a detection wavelength range of 400–1000 nm. The PL spectra were recorded using a spectrometer (tecSpec MMS) with a detection wavelength range of 400–1100 nm. A 405 nm laser was used as the excitation source. The temperature-dependent PL was obtained with VPF-100 liquid nitrogen cooled cryostat (Janis Research). The electrical characteristics were measured using a Keithley 2400 SourceMeter. The EL spectra, radiance, and EQE were recorded and calculated using a spectrometer (USB2000+, Ocean Optics) and ISM-Nit software (Isuzu Optics Corp.). The spectrometer was calibrated with a spectroradiometer (specbos 1211, JETI). Conventional transmission electron microscopy (TEM) observations were carried out using a JEOL JEM-2100 microscope.

3. Results and discussion

Fig. 1 shows the powder X-ray diffraction (XRD) patterns of the $CsSnBr_3$ and $CsSnI_3$ nanocrystals. The peak positions observed for the $CsSnBr_3$ and $CsSnI_3$ nanocrystals match well with the previous report, which confirmed that $CsSnBr_3$ and $CsSnI_3$ nanocrystals adopted the perovskite orthorhombic ($Pnma$) structure.[9] The prominent peaks observed at 14.4°, 25°, 28.7°, and 41.4° for $CsSnI_3$ correspond to the characteristic diffraction planes indexed at (101), (220), (202), and (242), respectively.[9,23] The prominent peaks observed at 15.2°, 21.6°, 30.8°, and 44.1° for $CsSnBr_3$ correspond to the characteristic diffraction planes indexed at (101), (121), (202), and (242), respectively.[9] The XRD patterns of the $CsSnI_3$ and $CsSnBr_3$ nanocrystals are in good agreement with the reference profile of orthorhombic $CsSnI_3$ (JCPDS file number: 43-1162) and cubic $CsSnBr_3$ (JCPDS file number: 70-1645). The inset of Fig. 1 shows the TEM images of the $CsSnBr_3$ and $CsSnI_3$ nanocrystals. The size of the $CsSnBr_3$ and $CsSnI_3$ nanocrystals are estimated to be about 25 and 7 nm, respectively. Due to the inability to get high resolution images, we are not able to get more detailed information.
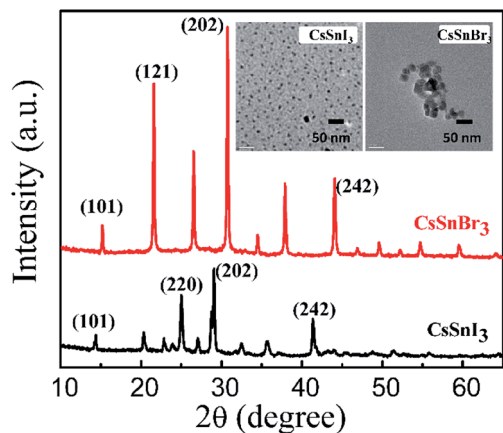
Fig. 1 Powder XRD patterns of CsSnBr₃ and CsSnI₃ perovskite nano-crystals. The insets show the TEM images of CsSnBr₃ and CsSnI₃ perovskite nanocrystals.

The UV-vis absorption and photoluminescence (PL) spectra of the CsSnBr₃ and CsSnI₃ nanocrystals were investigated, as shown in Fig. 2a and b. The insets in Fig. 2b are the photographs of CsSnBr₃ and CsSnI₃ nanocrystal suspensions under day light and UV light, respectively. The bandgaps of CsSnBr₃ and CsSnI₃ nanocrystals are roughly estimated to be 1.76 eV and 1.34 eV, respectively. By tuning the ratio of SnI_2 and $SnBr_2$ in the SnX_2–TOP solution using during the facile hot injection method, $CsSn(I_xBr_{1-x})_3$ nanocrystals can also be prepared. The absorption and PL spectra are shown in Fig. S1 and S2,† respectively. The onset of absorption shifts to higher energy while replacing I^- by Br^-. Such a bandgap tuning property is similar to the previous reports in $MASnX_3$, $MAPbX_3$, $CsSnX_3$, and $CsPbX_3$ material systems.[9,13,16,24–31] The PL spectra of the as-synthesized perovskite nanocrystals in solution showed an emission peak at 683 and 938 nm for CsSnBr₃ and CsSnI₃ nanocrystals, respectively.

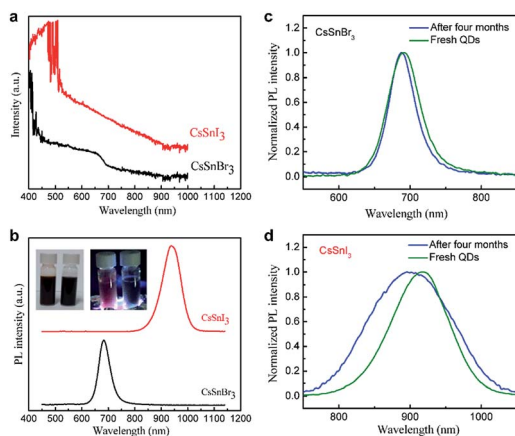The shelf stability of the CsSnBr₃ and CsSnI₃ nanocrystals in solution were also investigated, as shown in Fig. 2c and d. The CsSnBr₃ and CsSnI₃ nanocrystals suspensions were prepared and encapsulated in vials in the glove box. The vials were sealed and taken out of the glove box and stored in ambient condition for PL measurement. For CsSnBr₃ QDs, when comparing the fresh and four months stored solution, the PL peak was shifted from 683 nm to 681 nm, FWHM was increased from 50 nm to 55 nm, and the PL peak intensity was decreased from to 44.12% after 4 months. For CsSnI₃ QDs, the PL peak was shifted from 938 nm to 896 nm, FWHM was increased from 83 nm to 140 nm, and the PL peak intensity was decreased from to 15.26% after 4 months. The stability of CsSnBr₃ QDs solution is better than CsSnI₃ QDs solution (as shown in Fig. S3†). When the vial with CsSnI₃ nanocrystals suspension was opened, there will be no PL signal after six hours. This is supposed to be related to the spontaneous oxidative conversion from $CsSnI_3$ to Cs_2SnI_6.[32]

The steady-state PL spectra of CsSnBr₃ and CsSnI₃ nanocrystals in the temperature range between 80 K and 300 K are shown in Fig. 3a and b, respectively. With increasing the temperature, the PL peak shows a blue-shift tendency, the full width at half maximum (FWHM) of the PL spectra show

Fig. 2 (a) Absorption and (b) PL spectra of CsSnBr₃ and CsSnI₃ perovskite nanocrystals. Insets in (b) show the CsSnBr₃ and CsSnI₃ nanocrystals in day light and under UV light. The PL spectra of the fresh and aged (c) CsSnBr₃ and (d) CsSnI₃ perovskite nanocrystals.
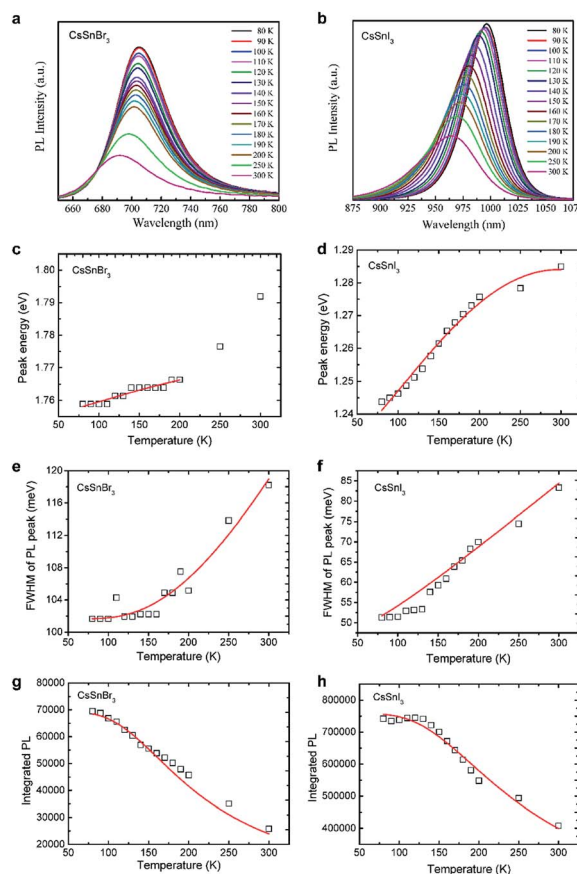

Fig. 3 (a and b) Temperature-dependent PL spectra, (c and d) PL peak energy, (e and f) FWHM of the PL spectra, and (g and h) PL integrated intensity of (a, c, e and g) CsSnBr₃ and (b, d, f and h) CsSnI₃ perovskite nanocrystals.

a broadening characteristics, and the integrated PL intensity shows a continuous decrease. All these behaviors were also observed in MAPbI$_3$, MAPbBr$_3$, FAPbI$_3$, FAPbBr$_3$, CsPbBr$_3$, CsPbI$_3$, CsSnI$_3$.[4,33–36] The temperature-dependent PL is worthy to be investigated in detail since important physical parameters of perovskites such as exciton binding energy, charge carriers–phonon interaction and band gap can be estimated.

The peak energy of the PL of CsSnBr$_3$ and CsSnI$_3$ nanocrystals as a function of temperature is shown in Fig. 3c and d. The peak energy increases with increasing the temperature. Such a blue-shift in PL peak energy cannot be described by a traditional empirical relation, $E_g = E_0 - \alpha T^2/(T + \beta)$,[37] which have been widely used to describe the temperature-dependent PL of conventional semiconductors. The empirical relation proposed by R. Pässler[38] and an expression which follows the Bose–Einstein statistical factor[39–41] are also not able to describe the blue-shift in PL peak energy.

The dependence of the band gap at constant pressure comprises two contributions. One contribution is due to the thermal expansion of the lattice (changes in lattice constant), and another contribution is the renormalization of band energies by electron–phonon interactions.[42–44] An expression was used to estimate the temperature-dependence of the band gap:[33,34]

$$\frac{\partial E_g}{\partial T} = \frac{\partial E_g}{\partial V}\frac{\partial V}{\partial T} + \sum_{j,\vec{q}}\left(\frac{\partial E_g}{\partial n_{j,\vec{q}}}\right)\left(n_{j,\vec{q}} + \frac{1}{2}\right), \quad (1)$$

where $n_{j,\vec{q}}$ is the occupation number of the phonon mode at j branch with wave vector $\vec{q}$. The first term in eqn (1) corresponds to the contribution of thermal expansion, while the second term is the contribution of electron–phonon interaction. Under the assumption of positive coefficient $\partial E_g/\partial V$[33] and one-oscillator mode,[33,45] eqn (1) can be simplified as follow:[33]

$$E_g(T) = E_0 + A_{TE}T + A_{EP}(2/(\exp(\hbar\omega/kT) - 1) + 1), \quad (2)$$

where E_0 is the unrenormalized band gap, $\hbar\omega$ is the average phonon energy. According to the fitting, the revealed parameters for CsSnBr$_3$ nanocrystals are $E_0 = 1.82$ eV and $\hbar\omega = 90.1$ meV, while the revealed parameters for CsSnI$_3$ nanocrystals are $E_0 = 1.76$ eV and $\hbar\omega = 100.3$ meV. For the fitting of CsSnBr$_3$ nanocrystals, since the deviation of PL peak energy is large, only the data below 200 K is used for fitting. These fitting results shown a good match, indicating the importance of the contribution of thermal expansion in these materials. For CsSnX$_3$ (X = I$^-$, Br$^-$, and Cl$^-$), the theoretical calculation has demonstrated that the band gap increases with increasing the lattice constant.[46] This also means that the thermal expansion leads to the increase in band gap. In conventional semiconductors, the thermal expansion contribution is negligible. However, in CsSnX$_3$, the thermal expansion contributes a lot.

As shown in Fig. 3e and f, the FWHM of the PL spectra broadens with increasing the temperature. The analysis on temperature-dependent PL broadening is a widely used method to understand the electron–phonon coupling in inorganic semiconductors.[5,33,35,36,47–49] Mechanisms related to the scattering between charge carriers and acoustic phonons, optical phonons or impurities have to be considered.[36,48] The following relation has been proposed to describe the evolution of FWHM with temperature:

$$\Gamma(T) = \Gamma_0 + \gamma_{ac}T + \gamma_{LO}/(e^{E_{LO}/kT} - 1) + \gamma_{imp}e^{-E_b/kT}, \quad (3)$$

The first term, Γ_0, is a temperature-independent inhomogeneous broadening. The second term is a homogeneous broadening, comes from acoustic scattering, while the third term is also a homogeneous broadening, results from LO phonon scattering. γ_{ac} is charge carrier–acoustic phonon coupling strength, and γ_{LO} is a charge carrier–optical phonon coupling strength. E_{LO} is the energy of the optical phonons. The final term is attributed to the scattering with ionized impurities with an average binding energy E_b. From the fitting process, the second and the fourth terms do not play any significant roles, and we only use the first and third term for theoretical fitting. According to the fitting, the revealed parameters for CsSnBr$_3$ nanocrystals are $\Gamma_0 = 101.6$ meV, $\gamma_{LO} = 158.6$ meV and $E_{LO} = 59.9$ meV, while the revealed parameters for CsSnI$_3$ nanocrystals are $\Gamma_0 = 45.4$ meV, $\gamma_{LO} = 28.6$ meV and $E_{LO} = 14.3$ meV.

The evolution of integrated PL intensity is shown in Fig. 3g and h, which shows a continuous decrease with increasing the temperature. This behavior is an indication that thermal energy activates exciton dissociation or nonradiative relaxation process, which compete with radiative recombination. The temperature-dependent PL intensity can be fitted to the Arrhenius law:[5,35,49–58]

$$I(T) = I_0/(1 + Ae^{-E_b/(kT)}), \quad (4)$$

where I_0 is the emission intensity at 0 K and E_b is the exciton binding energy or the activation energy of a non-radiative process. The fitting gives the value E_b of 48.8 meV for CsSnBr$_3$ nanocrystals, and E_b of 55.5 meV for CsSnI$_3$ nanocrystals.

To demonstrate the capability of perovskite nanocrystals to be used in the real application, near-infrared light-emitting diodes based on CsSnI$_3$ were realized. The device with a simple structure was adopted, that is ITO/PEDOT:PSS/emissive layer/LiF/Al. The emissive layer is a mixture composed of PVK, PBD, TPD, and CsSnI$_3$ nanocrystals. The optical and electrical properties of the device based on CsSnI$_3$ nanocrystals are shown in Fig. 4. The device with annealed emissive layer shown better performance than unannealed emissive layer. The maximum external quantum efficiently (EQE) of this device is about 0.007%. Such a low EQE value is attributed to the low quantum yield of the CsSnI$_3$ nanocrystals[9] and the leakage current. Considering the high electrical conductivity of CsSnI$_3$,[17] the leakage current may come from the percolation path in the emissive layer. Please note that there is no electroluminescence emission peak observed other than one belongs to the CsSnI$_3$. Therefore, we suppose that the charge carriers are transported mainly through the percolation path constructed by CsSnI$_3$ nanocrystals, and the electrons and holes are recombined on CsSnI$_3$. To further increase the efficiency of the device by reducing the leakage current, an electron
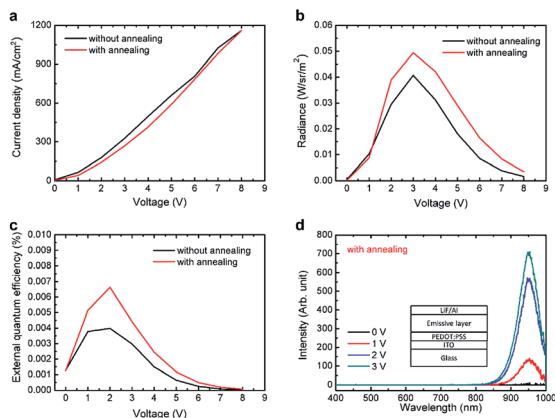
Fig. 4 Optical and electrical properties of the LEDs based on CsSnI$_3$. (a) Current density–voltage curves. (b) Radiance–voltage curves. (c) External quantum efficiency–voltage curves. (d) Electroluminescence spectra.

transport layer/hole blocking layer beneath the emissive layer and a hole transport layer/electron blocking layer above the emissive layer might be added.

In addition to use the perovskite nanocrystals in the emissive layer of the LED, we also use them to realize down-conversion color converter films. The color converter film was stacked on a blue LED (455 nm) for the down-conversion of blue light into the light with the wavelength of perovskite nanocrystals. The down-conversion color converter films were

Fig. 5 The characteristics of the color down-conversion films based on (a) CsSnBr$_3$/PMMA and (b) CsSnI$_3$/PMMA composite films.

prepared by blending the CsSnBr$_3$ or CsSnI$_3$ nanocrystals with PMMA host polymer. Fig. 5 shows the PL spectra of the CsSnBr$_3$/PMMA and CsSnI$_3$/PMMA composite films. A commercial blue LED with 455 nm emission was used as the excitation source. The PL spectra show peak values at ∼455 nm from the blue LED and the secondary peaks at 673 and 931 nm for CsSnBr$_3$/PMMA and CsSnI$_3$/PMMA composite films, respectively. These peak positions are similar to the ones of pure perovskite nanocrystals. CsSn(Br$_x$I$_{1-x}$)$_3$/PMMA composite films also works well for this demonstration, as shown in Fig S4.† These results demonstrated that a LED with emission wavelength range from 673 to 931 nm could be realized by stacking a down-conversion color converter film composed of CsSn(Br$_x$I$_{1-x}$)$_3$ and PMMA on a LED.

4. Conclusion

In summary, lead-free cesium tin halide CsSn(Br$_x$I$_{1-x}$)$_3$ nano-crystals were synthesized by a facile hot injection method. The sizes of CsSnBr$_3$ and CsSnI$_3$ nanocrystals are 25 and 7 nm, respectively. Temperature-dependent PL is used to unveil their exciton binding energy, charge carriers–phonon interaction and band gap. Light-emitting diodes based on CsSnI$_3$ and color down-conversion films based on CsSn(Br$_x$I$_{1-x}$)$_3$ were demonstrated.

Conflicts of interest

There are no conflicts to declare.

Acknowledgements

References

1 Z. Li, T. R. Klein, D. H. Kim, M. Yang, J. J. Berry, M. F. A. M. van Hest and K. Zhu, *Nat. Rev. Mater.*, 2018, **3**, 18017.

2 B. R. Sutherland and E. H. Sargent, *Nat. Photonics*, 2016, **10**, 295.

3 M. Kangzhe, D. Xiang-Yun, Z. Ya-Wen and C. Su, *J. Mater. Chem. C*, 2017, **5**, 9398.

4 H. Zhu, Y. Fu, F. Meng, X. Wu, Z. Gong, Q. Ding, M. V. Gustafsson, M. T. Trinh, S. Jin and X. Y. Zhu, *Nat. Mater.*, 2015, **14**, 636.

5 X. Li, Y. Wu, S. Zhang, B. Cai, Y. Gu, J. Song and H. Zeng, *Adv. Funct. Mater.*, 2016, **26**, 2435.

6 C. Yang, Y. Wu, Q. Ma and W. H. Zhang, *J. Energy Chem.*, 2018, **27**, 622–636.

7 X. He, Y. Qiu and S. Yang, *Adv. Mater.*, 2017, **29**, 1700775.

8 F. Liu, Y. Zhang, C. Ding, S. Kobayashi, T. Izuishi, N. Nakazawa, T. Toyoda, T. Ohta, S. Hayase, T. Minemoto, K. Yoshino, S. Dai and Q. Shen, *ACS Nano*, 2017, **11**, 10373–10383.
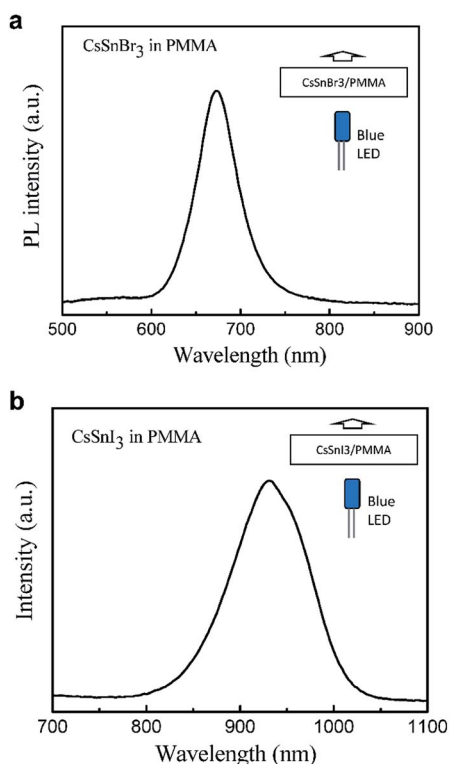
9   T. C. Jellicoe, J. M. Richter, H. F. J. Glass, M. Tabachnyk, R. Brady, S. E. Dutton, A. Rao, R. H. Friend, D. Credgington, N. C. Greenham and M. L. Böhm, *J. Am. Chem. Soc.*, 2016, **138**, 2941.

10 A. Wang, Y. Guo, F. Muhammad and Z. Deng, *Chem. Mater.*, 2017, **29**, 6493–6501.

11 A. B. Wong, Y. Bekenstein, J. Kang, C. S. Kley, D. Kim, N. A. Gibson, D. Zhang, Y. Yu, S. R. Leone, L. W. Wang, A. P. Alivisatos and P. Yang, *Nano Lett.*, 2018, **18**, 2060–2066.

12 F. Liu, C. Ding, Y. Zhang, T. S. Ripolles, T. Kamisaka, T. Toyoda, S. Hayase, T. Minemoto, K. Yoshino, S. Dai, M. Yanagida, H. Noguchi and Q. Shen, *J. Am. Chem. Soc.*, 2017, **139**, 16708–16719.

13 L. J. Chen, C. R. Lee, Y. J. Chuang, Z. H. Wu and C. Chen, *J. Phys. Chem. Lett.*, 2016, **7**, 5028.

14 I. Chung, B. Lee, J. He, R. P. H. Chang and M. G. Kanatzidis, *Nature*, 2012, **485**, 486.

15 M. H. Kumar, S. Dharani, W. L. Leong, P. P. Boix, R. R. Prabhakar, T. Baikie, C. Shi, H. Ding, R. Ramesh, M. Asta, M. Graetzel, S. G. Mhaisalkar and N. Mathews, *Adv. Mater.*, 2014, **26**, 7122.

16 D. Sabba, H. K. Mulmudi, R. R. Prabhakar, T. Krishnamoorthy, T. Baikie, P. P. Boix, S. Mhaisalkar and N. Mathews, *J. Phys. Chem. C*, 2015, **119**, 1763.

17 J. Zhang, C. Yu, L. Wang, Y. Li, Y. Ren and K. Shum, *Sci. Rep.*, 2014, **4**, 6954.

18 W. L. Hong, Y. C. Huang, C. Y. Chang, Z. C. Zhang, H. R. Tsai, N. Y. Chang and Y. C. Chao, *Adv. Mater.*, 2016, **28**, 8029.

19 K. Sasha and B. Yehonadav, *Nanoscale*, 2019, **11**, 8665.

20 V. Alessandro, P. Maddalena, B. Daniele, C. Carlo, Q. Paolo and M. Lorenzo, *Front. Chem.*, 2020, **8**, 35.

21 Y. Chonglong, C. Zhuo, J. W. Jian, P. William, V. Nemanja, T. K. John and S. Kai, *J. Appl. Phys.*, 2011, **110**, 063526.

22 H.-C. C. Oscar, Q. Tian, S. Matthew and H. S. Dong, *Nanoscale*, 2020, **12**, 13113.

23 I. Chung, J. H. Song, J. Im, J. Androulakis, C. D. Malliakas, H. Li, A. J. Freeman, J. T. Kenney and M. G. Kanatzidis, *J. Am. Chem. Soc.*, 2012, **134**, 8579.

24 F. Hao, C. C. Stoumpos, D. H. Cao, R. P. H. Chang and M. G. Kanatzidis, *Nat. Photonics*, 2014, **8**, 489.

25 N. K. Kumawat, A. Dey, A. Kumar, S. P. Gopinathan, K. L. Narasimhan and D. Kabra, *ACS Appl. Mater. Interfaces*, 2015, **7**, 13119.

26 J. H. Noh, S. H. Im, J. H. Heo, T. N. Mandal and S. I. Seok, *Nano Lett.*, 2013, **13**, 1764.

27 B. Suarez, V. Gonzalez-Pedro, T. S. Ripolles, R. S. Sanchez, L. Otero and I. Mora-Sero, *J. Phys. Chem. Lett.*, 2014, **5**, 1628.

28 S. A. Kulkarni, T. Baikie, P. P. Boix, N. Yantara, N. Mathews and S. Mhaisalkar, *J. Mater. Chem. A*, 2014, **2**, 9221.

29 G. Nedelcu, L. Protesescu, S. Yakunin, M. I. Bodnarchuk, M. J. Grotevent and M. V. Kovalenko, *Nano Lett.*, 2015, **15**, 5635.

30 L. Protesescu, S. Yakunin, M. I. Bodnarchuk, F. Krieg, R. Caputo, C. H. Hendon, R. X. Yang, A. Walsh and M. V. Kovalenko, *Nano Lett.*, 2015, **15**, 3692.

31 Q. A. Akkerman, V. D'Innocenzo, S. Accornero, A. Scarpellini, A. Petrozza, M. Prato and L. Manna, *J. Am. Chem. Soc.*, 2015, **137**, 10276.

32 X. Qiu, B. Cao, S. Yuan, X. Chen, Z. Qiu, Y. Jiang, Q. Ye, H. Wang, H. Zeng, J. Liu and M. G. Kanatzidis, *Sol. Energy Mater. Sol. Cells*, 2017, **159**, 227.

33 K. Wei, Z. Xu, R. Chen, X. Zheng, X. Cheng and T. Jiang, *Opt. Lett.*, 2016, **41**, 3821.

34 C. Yu, Z. Chen, J. J. Wang, W. Pfenninger, N. Vockic, J. T. Kenney and K. Shum, *J. Appl. Phys.*, 2011, **110**, 063526.

35 H. Diab, G. Trippé-Allard, F. Lédée, K. Jemli, C. Vilar, G. Bouchez, V. L. R. Jacques, A. Tejeda, J. Even, J. S. Lauret, E. Deleporte and D. Garrot, *J. Phys. Chem. Lett.*, 2016, **7**, 5093.

36 A. D. Wright, C. Verdi, R. L. Milot, G. E. Eperon, M. A. Pérez-Osorio, H. J. Snaith, F. Giustino, M. B. Johnston and L. M. Herz, *Nat. Commun.*, 2016, **7**, 11755.

37 Y. Varshni, *Physica*, 1967, **34**, 149.

38 R. Pässler, *Phys. Status Solidi B*, 1997, **200**, 155.

39 L. Viña, S. Logothetidis and M. Cardona, *Phys. Rev. B: Condens. Matter Mater. Phys.*, 1984, **30**, 1979.

40 S. Logothetidis, L. Via and M. Cardona, *Phys. Rev. B: Condens. Matter Mater. Phys.*, 1985, **31**, 947.

41 P. Lautenschlager, M. Garriga, S. Logothetidis and M. Cardona, *Phys. Rev. B: Condens. Matter Mater. Phys.*, 1987, **35**, 9174.

42 P. B. Allen and M. Cardona, *Phys. Rev. B: Condens. Matter Mater. Phys.*, 1983, **27**, 4760.

43 P. Lautenschlager, P. B. Allen and M. Cardona, *Phys. Rev. B: Condens. Matter Mater. Phys.*, 1985, **31**, 2163.

44 A. Göbel, T. Ruf, M. Cardona, C. T. Lin, J. Wrzesinski, M. Steube, K. Reimann, J. C. Merle and M. Joucla, *Phys. Rev. B: Condens. Matter Mater. Phys.*, 1998, **57**, 15183.

45 J. Bhosale, A. K. Ramdas, A. Burger, A. Muñoz, A. H. Romero, M. Cardona, R. Lauck and R. K. Kremer, *Phys. Rev. B: Condens. Matter Mater. Phys.*, 2012, **86**, 195208.

46 L. Huang and W. R. L. Lambrecht, *Phys. Rev. B: Condens. Matter Mater. Phys.*, 2013, **88**, 165203.

47 S. Rudin, T. L. Reinecke and B. Segall, *Phys. Rev. B: Condens. Matter Mater. Phys.*, 1990, **42**, 11218.

48 J. Lee, E. S. Koteles and M. O. Vassell, *Phys. Rev. B: Condens. Matter Mater. Phys.*, 1986, **33**, 5512.

49 Z. F. Shi, X. G. Sun, D. Wu, T. T. Xu, Y. T. Tian, Y. T. Zhang, X. J. Li and G. T. Du, *J. Mater. Chem. C*, 2016, **4**, 8373.

50 K. Wu, A. Bera, C. Ma, Y. Du, Y. Yang, L. Li and T. Wu, *Phys. Chem. Chem. Phys.*, 2014, **16**, 22476.

51 S. Sun, T. Salim, N. Mathews, M. Duchamp, C. Boothroyd, G. Xing, T. C. Sum and Y. M. Lam, *Energy Environ. Sci.*, 2014, **7**, 399.

52 T. J. Savenije, C. S. Ponseca Jr, L. Kunneman, M. Abdellah, K. Zheng, Y. Tian, Q. Zhu, S. E. Canton, I. G. Scheblykin, T. Pullerits, A. Yartsev and V. Sundström, *J. Phys. Chem. Lett.*, 2014, **5**, 2189.

53 S. M. Lee, C. J. Moon, H. Lim, Y. Lee, M. Y. Choi and J. Bang, *J. Phys. Chem. C*, 2017, **121**, 26054.

54 A. Yangui, S. Pillet, A. Mlayah, A. Lusson, G. Bouchez, S. Triki, Y. Abid and K. Boukheddaden, *J. Chem. Phys.*, 2015, **143**, 224201.

55 J. Fujisawa and T. Ishihara, *Phys. Rev. B: Condens. Matter Mater. Phys.*, 2004, **70**, 205330.

56 D. S. Jiang, H. Jung and K. Ploog, *J. Appl. Phys.*, 1988, **64**, 1371.

57 X. Hong, T. Ishihara and A. V. Nurmikko, *Phys. Rev. B: Condens. Matter Mater. Phys.*, 1992, **45**, 6961.

58 T. Ishihara, J. Takahashi and T. Goto, *Phys. Rev. B: Condens. Matter Mater. Phys.*, 1990, **42**, 11099.